Recent advances in sailing yacht aerodynamics

Citation for published version:
Viola, IM 2013, 'Recent advances in sailing yacht aerodynamics' Applied Mechanics Reviews, vol. 65, no. 4, 040000, pp. 1-12. DOI: 10.1115/1.4024947

Digital Object Identifier (DOI):
10.1115/1.4024947

Document Version:
Early version, also known as pre-print

Published In:
Applied Mechanics Reviews

Recent Advances in Sailing Yacht Aerodynamics

Ignazio Maria VIOLA

Abstract

The analysis of sailing yacht aerodynamics has changed dramatically over the last 15 years and has enabled significant advances in performance prediction. For instance, the growth of Computational Fluid Dynamics has significantly changed the way high performance sails are designed. Three-dimensional mathematical models of fully rigged sail plans, and the visualisation of the turbulent unsteady flow pattern around them, are now quite common whereas ten years ago such a simulation would have been very rare, and twenty years ago impossible. The parallel development of optimisation techniques has resulted in new sail and yacht design methods. Changes in the experimental techniques have been as dramatic as in the numerical techniques. The introduction of the Twisted Flow Device, the Real-Time Velocity Prediction Program and the most recent pressure measurements, has allowed a step change in the potentialities of experimental sail aerodynamics. This paper aims to reviewing the recent advances in sail aerodynamics and to highlight potential research areas for future work.

Keywords

Sail aerodynamics; yacht; wind tunnel test; full-scale test; pressure measurement; thin airfoil; laminar separation bubble; trailing edge separation.

Outline

1. INTRODUCTION

1.1 SAILING COMPETITIONS

Major advancements in the study of sail aerodynamics in the last 100 years has been motivated by the research performed for a small number of high profile yacht races. The two most important of them summarised below.

The America's Cup (AC) is the oldest sporting trophy in the world and was sailed for the first time in 1852 around the Isle of Wight, UK. Since then, the AC has been sailed at irregular intervals of several years. In recent years, a typical challenger will invest approximately £100 million over a period of 2-4 years to design and build a new yacht and train the crew how to sail. The AC competition itself is a *match race* (i.e. a one-on-one race between the challenger and the defender), sailed along a windward-leeward course. A critical part of the race is the first windward leg, where the yachts sail at close wind angles in order to reach an upwind buoy. Therefore, until the most recent AC in 2010, America's Cup Class (ACC) yachts were optimised to perform particularly well in light-wind upwind conditions (i.e. in the first leg of the race). The most recent yacht sailed was between a catamaran with conventional flexible sails, and a trimaran with the largest rigid wing ever built. Her wing was 68 m long; in comparison the wing of an Airbus A380 is 'only' 43.5 m. These catamarans must perform well in a wider range of wind conditions, and their manoeuvrability in a strong breeze is crucial.

The Volvo Ocean Race (VOR), formerly known as the Whitbread Round the World Race, is the most prestigious long distance ocean yacht race and is sailed every 3-4 years. The yachts sail about ten port-to-port legs which takes them all around the world. Each leg can take up to ten days and the wind conditions vary from very light airs near the equator to very strong breezes at the highest latitudes. Most of the race is sailed in the same direction as that of the main wind directions, i.e. downwind conditions, and the yachts are lighter and significantly faster than the ACC yachts. A critical constraint for the race is the maximum number of sails allowed on board, which is very limited compared to the variety of encountered wind conditions. This means that the sails cannot be optimised for a specific wind direction, wind speed and wave condition as in the AC. Therefore, a careful analysis of the crossovers between the sail optimum ranges and the estimated hours of utilisation needs to be performed.

1.2 SAILS

Sails are thin flexible membranes which are trimmed by a yacht crew to an optimum shape and direction for each wind condition. Optimising the sail shape and trim is a highly important skill and involves the adjustment of numerous controls attached to the sail and the supporting rig (the mast and stays). On modern sloop rigged racing yachts there are three types of sails: mainsail, headsail and spinnaker. The mainsail is used in every condition together with one of the two other sails. The headsail is mainly used when the yacht is sailing upwind, i.e. when the angle between the wind direction and the yacht heading is smaller than 90°. The two most common headsails are the genoa and the jib, and genoas are typically larger than jibs. Conversely, the spinnaker is used when the yacht is sailing downwind, i.e. when the angle between the wind direction and the yacht heading is greater than 90°. Most modern racing yachts sail asymmetric spinnakers, whilst for cruising yachts symmetric spinnakers are more popular.

The leading edge of the mainsail is attached to the mast and the bottom edge to the boom. The sail is trimmed by moving the position of the bottom corner of the trailing edge, namely the *clew* (Fig.

1), and also adjusting several other controls attached to the sail and rig. Trimming the clew position directly changes the sail performance by altering the angle of attack to the wind and also induces bending of the mast, which has a significant effect on the sail shape. The headsail is attached to the *forestay*, a wired cable connecting the top of the mast to the yacht's bow, and it is trimmed principally by moving the position of its clew. The spinnaker (Fig. 2) has only three fixed corners and is trimmed by positioning the two lower clews. The spinnaker trim is further controlled by a pole, which is attached to the windward clew at one end, and the mast at the other.

1.3 WIND TRIANGLE

A yacht sails in the atmospheric boundary layer, namely *true wind* (Fig. 3). The wind experienced by a yacht, namely *apparent wind*, is the vectorial difference between the true wind and the boat velocity. The supplementary angle between the apparent wind velocity and the boat velocity is termed the *apparent wind angle* (AWA). On the lowest sections of the sail, the AWA is lower than on the highest sections. The direction variation of the apparent wind angle is the *apparent wind twist*.

1.4 EQUILIBRIUM OF A SAILING YACHT

When a yacht sails at a constant velocity, the vectorial sum of all the forces acting upon it must be zero. The velocity of a yacht can thus be computed by determining the equilibrium of these forces. This principle is the basis for the Velocity Prediction Program (VPP), which is used to design a yacht hull and in some cases, the sails too. The architecture of most of the modern VPP's is well described by Claughton *et al.* [1] and Larsson and Eliasson [2], while more technical details can be found in Van Oossanen [3]. Similar programs are also used to design and optimise wind-driven terrestrial vehicles (for instance, see ref. [4]), though without the need to model the complex hydrodynamic behaviour and the free surface effects.

The inputs to the VPP are the hydrodynamic characteristics of the hull and the aerodynamic characteristics of the sails. The hydrodynamic inputs include the resistance of the hull as a function of boat speed and the righting moment as a function of heel angle. The aerodynamics is defined principally by *sail coefficients,* which describe the forces and moments generated from the sails. The three force components are in the direction of the boat velocity, F_x, the sway direction, F_y, and the vertical heave direction, F_z. These are divided by the far field dynamic pressure q_∞ and the sail area S in order to define the three force coefficients in Eq. (1), where dynamic pressure is defined as $q_\infty = ½\, \rho V_\infty{}^2$, ρ is the density and V_∞ the far field velocity of the air.

$$C_x = \frac{F_x}{q_\infty\, S};\; C_y = \frac{F_y}{q_\infty\, S};\; C_z = \frac{F_z}{q_\infty\, S} \qquad (1)$$

Moments produced by the sails (M_x, M_y, M_z) are divided by q_∞, S, and a reference length, such as for instance $\sqrt{S}$, in order to define the three moment coefficients in Eq. (2).

$$C_{M_x} = \frac{M_x}{q_\infty\, S\, \sqrt{S}};\; C_{M_y} = \frac{M_y}{q_\infty\, S\, \sqrt{S}};\; C_{M_z} = \frac{M_z}{q_\infty\, S\, \sqrt{S}} \qquad (2)$$

If a reference AWA is chosen, for example the AWA at a height of 10 m, then the wind axis can be defined. Usually the lift L (defined on the horizontal plane) and the drag D are divided by q_∞ and S in order to define the coefficients in Eq. (3).

$$C_L = \frac{L}{q_\infty S};\ C_D = \frac{D}{q_\infty S} \tag{3}$$

The sails are trimmed in order to achieve the maximum boat velocity for every AWA. Unfortunately, there is not a constant correlation between the optimum sail trim and the sail coefficients. In fact, the trim that produces the maximum drive force (F_x), might lead to an unacceptably large side force (F_y) and heeling moment (M_x). The aerodynamic side force must be equilibrated by the hydrodynamic side force. The latter is achieved by a leeway angle allowing an angle of attack on the appendages, which provides the needed lift. The hydrodynamic lift implies a drag due to lift; therefore, increasing the aerodynamic side force leads to additional hydrodynamic drag. Similarly, the heeling moment causes the boat to heel, which can cause an increase in hull resistance. Therefore, the trim of the sail allowing the maximum drive force is often different from the one allowing the maximum boat speed.

In upwind conditions, the aerodynamic drag has a negative component along the boat velocity direction and thus it should ideally be low. Conversely, in downwind conditions it has a positive component and thus it can be higher. Therefore, in upwind conditions the sail coefficients, which allow the optimum velocity, have high C_x/C_y and C_L/C_D ratios, while in downwind conditions they have a high C_x and C_L.

The sail coefficients that produce the maximum boat speed are chosen by the VPP, which explores several possible equilibrium conditions and selects the condition with the highest boat speed. Therefore, to perform satisfactorily, the VPP needs a reliable set of possible sail coefficients as the input.

2. WIND TUNNEL TESTS

Sail coefficients can be derived from wind tunnel tests or Computational Fluid Dynamics (CFD). The main advantage of the numerical approach is the possibility of integrating the aerodynamic analysis into the design process and numerical codes can be easily integrated into the VPP. However, as shown in Section 2.4, a new wind tunnel technique developed in 2003 integrates the wind tunnel tests into the VPP via a hardware-in-the-loop method. Also, the CFD must be coupled to a structural code to compute the displacement of the sail, and the accuracy of the coupled CFD-structural code is still not yet fully understood.

Wind tunnel tests have the advantage that flexible sails can be used and the sails can be trimmed as in a full scale yacht. The sails can be made of the same materials as for a full scale yacht but using thinner cloths. They can be trimmed with sheets pulled by remotely controlled drums thus simulating the actions of the yacht crew. A six-component balance placed below or inside the yacht model is used to measure the forces and whilst sails are trimmed, the aerodynamic forces are monitored. When a sail trim is selected, the forces are measured for several seconds and averaged values are used to compute the sail coefficients. Further discussion about the advantages of investigating sail aerodynamics with wind-tunnel tests, full-scale tests or numerical methods can be found in ref. [5].

2.1 SCALING PROBLEMS

In order to achieve a scaled representation of the full-scale flow field, the ratio between inertial and viscous forces of the flow should be the same in the wind tunnel and in full-scale. This ratio, namely the Reynolds number, is defined in Eq. (4), where υ is the kinematic viscosity of the air.

$$Re = \frac{V_\infty \sqrt{S}}{\upsilon} \tag{4}$$

Assuming a geometrical scale λ defined in Eq. (5), with $\lambda > 1$, the model-scale velocity must obey Eq. (6) in order to allow the same Re in model-scale ($_{MS}$) and full-scale ($_{FS}$) conditions.

$$\left(\sqrt{S}\right)_{MS} = \frac{1}{\lambda}\left(\sqrt{S}\right)_{FS} \tag{5}$$

$$(V)_{MS} = \lambda (V)_{FS} \tag{6}$$

The strain in the rigging ε_{rig} is proportional to the stresses σ_{rig} through Young's modulus E_{rig}. In turn, the stresses are proportional to the dynamic pressure q_∞.

$$\varepsilon_{rig} \propto \frac{\sigma_{rig}}{E_{rig}} \propto \frac{q_\infty}{E_{rig}} \propto \frac{\rho\, {V_\infty}^2}{E_{rig}} \tag{7}$$

Therefore, the Young's modulus of the model-scale rigging should obey Eq. (8) in order to allow the strain to be modelled correctly.

$$\left(E_{rig}\right)_{MS} = \lambda^2 \left(E_{rig}\right)_{FS} \tag{8}$$

Unfortunately, masts of modern yachts are already built with high modulus materials and it is not possible to find materials with a much higher modulus. Therefore, in order to preserve the model integrity, the model-scale velocity is almost the same as the full-scale velocity, leading to a lower model-scale Re than the full-scale Re.

For example, the sail area of an ACC yacht is about 800 m^2 in full scale and 3.5 m^2 in a 1:15th model scale, whilst the wind velocity ranges between 5 and 15 knots ($2.6 - 7.7$ m/s) both for the full and model scales, leading to Re of the order of 10^7 in full-scale conditions and 10^5 in model-scale conditions. Testing at 7.7 m/s in the wind tunnel is equivalent to 0.5 m/s for a full-scale yacht.

The error due to the reduced Re has never been quantified. There is an argument that suggests that a Re difference of one or two orders of magnitude is sufficiently small in turbulent atmospheric wind flow so as to produce a negligible error. However, a converse argument suggests that the laminar to turbulent transition plays a fundamental role in the suction near the leading edge of the sail, which is the region proving most of the driving force. Thus the scaling error has a significant effect on the solution accuracy. Several authors (for instance, see ref. [6]) have tried to quantify this difference by modelling the same conditions for the model and full-scale Re with CFD. However, the higher Re leads to a thinner boundary layer, thus the grid resolution plays a significantly different role for the two Re values. It can be shown that scaling the grid for the two Re would require an unreachable number of grid points. Therefore, quantifying the effect of the different Re has not been possible until now.

A spinnaker is attached to a yacht rig at its three corners only. Therefore, the flying shape of the spinnaker is significantly affected by the ratio between aerodynamic forces, which inflates the sail, and the gravitational force, which tends to deflate it. This ratio, which is expressed in Eq. (9) through the sail's Froude number, Fr_{sail} , should be equal in model-scale and full-scale conditions.

$$Fr_{sail}{}^2 = \frac{\rho\, V_\infty{}^2 S}{m\, g} = \frac{\rho\, V_\infty{}^2 S}{\rho_s\, t\, S\, g} = \frac{\rho}{\rho_s}\,\frac{V_\infty{}^2}{t\, g} \tag{9}$$

where m, t and ρ_s are the mass, thickness and density of the sail, respectively.

The strain in the spinnaker cloth can be computed by considering that the sail is equivalent to a thin membrane. The sail's normal stresses σ_{sail} are proportional to the strain ε_{sail} through the Young's modulus E_{sail}. Therefore, an equation similar to Eq. (7) for the rigging can be written for the sails. However, it is common practice to violate the geometrical similitude and to change the ratio between the thickness and the area of the sail. Therefore, ε_{sail} is expressed in Eq. (6) using the sail's cross-section area A.

$$\varepsilon_{sail} \propto \frac{q_\infty S}{E_{sail} A} \propto \frac{\rho\, V_\infty{}^2 S}{E_{sail}\, t\, \sqrt{S}} = \frac{\rho\, V_\infty{}^2}{E_{sail}}\frac{\sqrt{S}}{t} \tag{10}$$

The model-scale sailcloth must obey Eqs. (11-12), which take into account that Fr_{sail} and ε_{sail}, respectively, must be the same in model-scale and full-scale conditions.

$$(\rho_s t)_{MS} = \lambda^2 (\rho_s t)_{FS} \tag{11}$$

$$(E_{sail} t)_{MS} = \lambda (E_{sail} t)_{FS} \tag{12}$$

Eqs. (11-12) show that, if the velocity were scaled with Eq. (6), a heavier and more resistant material should be used in wind tunnel tests than for a full scale yacht. However, these are ideal conditions, which cannot be achieved due to the limitation in the maximum wind speed sustainable by the model. As a consequence, these equations should be rewritten considering a velocity scale $\lambda_V \leq \lambda$:

$$(V_\infty)_{MS} = \lambda_V (V_\infty)_{FS} \tag{13}$$

$$(\rho_s t)_{MS} = \lambda_V{}^2 (\rho_s t)_{FS} \tag{14}$$

$$(E_{sail} t)_{MS} = \frac{\lambda_V{}^2}{\lambda} (E_{sail} t)_{FS} \tag{15}$$

In downwind conditions, where large sail areas are carried by the yacht, λ_V is less than 1. In this situation, Eqs. (14-15) show that a lighter and less resistant material should be used in wind tunnel tests than for a full scale yacht. In particular, model-scale spinnakers are usually made of the same cloth as for a full-scale yacht but of a lower thickness. This is considered a reasonable approximation if the thickness is reduced by more than a factor of $\frac{\lambda_V{}^2}{\lambda}$ and less than a factor of $\lambda_V{}^2$.

2.2 TESTING PROCEDURE

A detailed model of a yacht is used for wind tunnel tests, with as many features as possible included. For instance, the crew are modelled to take into account the interaction with the flow passing between the sail and the hull. A balance below or inside the model measures the aerodynamic forces and this has 6 load cells, one along the $\boldsymbol{X}$-direction, two along the $\boldsymbol{Y}$-direction and three along the $\boldsymbol{Z}$-direction. This is because the uncertainty is minimum in the $\boldsymbol{X}$-direction and maximum in the $\boldsymbol{Z}$-direction. The direction with lowest uncertainty is used to measure the drive force F_x, while the maximum uncertainty is used to measure the vertical force F_z.

An initial zero-wind measurement is performed just before the test commences. Following this, the wind is directed at the model and the sails are remotely trimmed. For several trims, forces are measured for 20 to 90 seconds (depending on the particular wind tunnel) in order to take into account possible low frequency wind speed fluctuations, and averaged values are computed. Every 20-40 minutes the wind is stopped and a final zero-wind measurement is performed in order to take into account of the variation in the load-cells force readings due to the temperature variations during the test. In order to take this effect into account, a linear correction is applied using the initial and the final zero-wind measurements.

F_x and F_y can be transformed into coefficients, C_x and C_y, using Eq. (1). Therefore, for each wind condition, the full-scale forces can be computed by multiplying the coefficients for the full-scale dynamic pressure and sail area. The aim of the testing procedure is to determine the maximum C_x, for a range of C_y. In fact, for a given C_y, the highest C_x allows the highest boat velocity. The same C_x can be achieved through two trims with two different values of C_y, and the trim with the lower C_y enables the higher boat velocity.

Figure 4 shows C_x versus C_y for eight different trims in upwind conditions. These eight trims can be measured in about 20 minutes. The sails are initially trimmed in order to determine the maximum C_x with no regard for C_y. Then the mainsail is over-trimmed (moving the mainsail traveller upwind) which leads to a lower C_x and a higher C_y. The mainsail is then de-powered (initially easing the traveller and then easing the sheet) leading to a lower C_x and C_y. When the mainsail is largely depowered, lower upwash occurs on the headsail, which can be trimmed in to increase the angle of attack.

In light wind conditions, a high C_y usually leads to a low full-scale side force. In this condition, the trim producing the maximum C_x also produces the maximum boat speed. Conversely, in a strong breeze, a high C_y leads to a high full-scale side force, which significantly increases the hydrodynamic resistance. In this condition a trim with lower C_x and C_y produces a higher velocity. Therefore, the sail trim allowing the maximum speed in light air is correlated with a trim on the right in Fig. 4, while in a strong breeze it is correlated with a trim on the left in Fig. 4.

The same results can be rotated from body axes to wind axes. Figure 5 shows the lift and drag coefficients for the eight sail trims presented in Fig. 4. It is interesting to note that, in upwind conditions, the trim leading to the maximum C_x has a lower lift coefficient then the maximum one.

The drag force coefficient can be split into three components: parasitic (C_{D_p}), induced (C_{D_i}) and separation (C_{D_s}), where the last two components depend on C_L. The second component is due to irrotational flow, while the first and third components are due to viscous effects.

$$C_d = C_{D_p} + C_{D_i}(C_L) + C_{D_s}(C_L) \quad (16)$$

Figure 6 shows that most of the trims lie on a straight line on a plot of C_D versus ${C_L}^2$. The intercept of the line with the zero-lift axis is C_{D_p}. Assuming an elliptical planform, C_{D_i} increases linearly with ${C_L}^2$.

$$C_{D_i} = \left(\frac{1}{\pi\ AR}\right){C_L}^2 = \left(\frac{S}{\pi b^2}\right){C_L}^2 \quad (17)$$

where AR and b are the aspect ratio and the span of an equivalent elliptical sail plan, respectively.

Figure 6 shows that the sum of C_{D_i} and C_{D_s} increases almost linearly with ${C_L}^2$ for loose trims. Eq. (17) shows that C_{D_i} increases linearly with ${C_L}^2$. Therefore, also C_{D_s} must increase linearly with ${C_L}^2$.

Most of the VPP's assume that C_{D_s} is negligible. Therefore, the inputs are C_L and C_D of the trim giving the maximum drive force, C_{D_p} and the span of the equivalent elliptic sail plan computed from the slope of the line in Fig. 6. It should be noted that this can lead to an incorrect estimate of the drag because the trim allowing the maximum drive force is not in the linear range of Eq. (16). Examples of modern aerodynamic coefficients can be found in ref. [7], while examples of how a sailing rig is optimised with wind tunnel tests can be found in ref. [8].

The lift and drag are corrected to take into account the aerodynamic forces, namely *windage*, which is due to the hull, mast and other appendages. These forces are measured for the model when the sails are absent and are subtracted from the forces measured with the sails. However, this technique introduces a significant error because it does not take into account of the interactions between the sails, the mast and the hull.

The procedure presented in this Section is used to perform tests in upwind conditions. In downwind conditions various procedures can be performed, though these procedures are all based on the presented principles. It should be noted that, for the same drive force, the higher the AWA the lower the side force. Therefore, at very high AWA only the trim giving the maximum drive force is relevant.

2.3 TWISTED FLOW DEVICE

As mentioned above, the yacht experiences a vertical wind profile, which varies both in speed and direction (twist) from the water plane to the top of the mast. The change in direction increases with the apparent wind angle. Therefore, it is significant in downwind conditions, while it can be neglected in upwind conditions.

At the Twisted Flow Wind Tunnel of the Yacht Research Unit (YRU), which has a 7m-wide and 3.5m-high test section, a boundary layer develops for 13.5 m downstream from the last screen of the fan (used to make the flow uniform). The boundary layer profile is modified using horizontal bars across the section in order to slow and change the characteristics of the flow. In 1996, Flay [9] introduced a twisted flow device to also model the vertical profile of the apparent wind angle. It was found that this device significantly increased the agreement between wind-tunnel results and full-scale observations.

Before 1996, downwind sails had to be trimmed differently in existing straight-flow wind tunnels compared to on full-scale yachts. Today, it is common practice to model downwind sails with a twist device and upwind sails without a twist device. In fact, the twist of the wind profile can be neglected in upwind conditions, where the deflection is of the order of 1° along the sail span, while it cannot be neglected in downwind conditions where the deflection is much higher and vary significantly for different boat types and AWA's. For example, it can vary by 10° on a 10-m cruiser/racer yacht sailing at AWA = 40°, and by 35° on a high-performance 60′-long VO60-class yacht sailing at AWA = 160° [10].

The twisted flow device increases the angle of attack on the highest sections and decreases it on the lowest sections, while the flow is not deflected at a reference height (typically 10m in full-scale), where the nominal AWA is computed. Surprisingly, testing with the twisted flow device leads to higher aerodynamic forces both on the highest and the lowest sections of the sails [11]. As a consequence, sails were found to allow higher aerodynamic forces when trimmed in twisted flow conditions than in uniform flow, proving that the twist of the onset flow wind velocity has a positive and non negligible effect on sails.

Following the New Zealand example, twisted flow devices were introduced into three European wind tunnels; at the Politecnico di Milano Wind Tunnel [12], at the Twisted Flow Wind Tunnel of the YRU of the University of Applied Sciences Kiel, Germany [13], and at the wind tunnel used by BMW Oracle Racing, challenger for the 32nd America's Cup, in Valencia, although this was dismantled at the end of the race. Today, the three remaining twisted flow wind tunnels are the most important wind tunnels for sail aerodynamics. Details on these facilities are provided in Section 2.7.

The devices are all based on similar concepts. The twist is introduced by an array of vertical thin vanes which run from the floor to the roof and are placed a few metres upstream from the model. The vanes are twisted in order to deflect the wind on the lowest section in one direction and on the highest section in the opposite direction. For instance, in Fig. 2, the twisted flow device designed by the author for the Politecnico di Milano Wind Tunnel can be seen upstream of the model, and this device is the largest of its type. Figure 7 shows the white vanes adopted at the Twisted Flow Wind Tunnel in Auckland and Fig. 8 shows the vanes adopted at the Twisted Flow Wind Tunnel in Kiel.

These devices are design to allow a wide range of vertical wind twist profiles. The good correspondence between the wind profile measured at the test section and the target wind profile, which is computed by the vectorial sum of a logarithmic atmospheric boundary layer with the boat velocity, can be found for example in refs. [14,15]. The major limitation of the twisted flow device is that the yacht model is tested in the wake of the vanes. The vanes are very thin and short and, if well trimmed, the flow is attached along the whole chord [15]. However, even if the resulting wakes are quite thin, these are still noticeable at the test section and their effect is unknown.

The twist device allows modelling the time-averaged apparent wind velocity experienced buy the sailing yacht. However, the dynamic variations of the onset wind due to the turbulence of the atmospheric boundary layer and the dynamics of the yacht are modelled with difficulty in wind tunnels. Recent experiments aiming at modelling the yacht motion are discussed in Section 2.6, while the effect of different turbulent characteristics of the onset flow on the aerodynamic forces is still largely unknown. The motion of a yacht changes the encounter frequency with the wind fluctuations [16,17], leading to a shift of the wind spectrum peak towards higher frequencies when sailing upwind and towards lower frequencies when sailing downwind, while the peak amplitude remains constant. Moreover, the helmsman acts as a lower band filter while steering the yacht according to the wind shifts at full scale. Therefore, the wind spectrum should be set together with the wind profile for every tested condition, something that is still practically impossible. Interested readers can find more details in ref. [7]. Usually, a turbulence intensity of around 5% and turbulent length scales of the order of 0.1 m are used in wind tunnels as those presented in Section 2.7.

2.4 REAL-TIME VPP

In 2003, the YRU in Auckland introduced a second breakthrough: a Real-Time VPP [18]. Today, it is estimated that the YRU performs more than two-thirds of the yacht sail wind tunnel tests in the world, and it performs most of them using the Real-Time VPP. This allows testing in a free-to-heel condition, where the hydrodynamic righting moment is computed by the VPP and the associated heel is mechanically applied in real time. In 2006, the Politecnico di Milano Wind Tunnel built a similar device [19]. The BMW Oracle wind tunnel in Valencia was also equipped with a Real-Time VPP, while the Twisted Flow Wind Tunnel in Kiel does not have such a capability.

The Real-Time VPP allows improvement of the testing procedure presented in Section 2., where a set of trims is tested for several AWA's and heel angles, and different sail trims are considered in order to maximise the drive force in a range of side forces. Firstly, the Real-Time VPP allows trimming of the sails for the maximum boat speed instead of the maximum drive force. Hansen *et al.* [18] showed that optimising the sail trim for the maximum boat speed can lead to boat speeds up to 1% higher than when the sails are optimised for the maximum drive force. Secondly, the Real-Time VPP does not assume a linear correlation between C_d and C_l^2, which neglects the separation drag as showed in Section 2.2. In fact, the trim effect is not modelled and the aerodynamic forces are measured for every optimum trim. Finally and very importantly, enabling testing of every trim with its correlated heel allows testing only realistic trims, decreasing significantly the total number of tests to be performed.

On the other hand, this testing procedure leads to higher measurement uncertainty than the fixed-heel procedure presented in Section 2.2, and also requires a more experienced operator to find the trim allowing the maximum boat speed. Therefore, this procedure is suitable for testing downwind sails, where the sail coefficients are less sensitive to the trim, while the fixed-heel procedure is more suitable for testing upwind sails.

As mentioned above, the net aerodynamic forces due to the sails are obtained by subtracting the windage from the measured forces. This rough approximation is unnecessary when the Real-Time VPP is used because differently from a conventional VPP, it uses the aerodynamic forces acting on the whole model.

This technique was also used as a research tool to investigate how the sail trim was taken into account by the aerodynamic models implemented in conventional VPP's [18]. This research led to new aerodynamic models where the accuracy in modelling the force changes due to different trims was enhanced. In particular, Hansen *et al.* [20] proposed the use of the parameters 'twist' and 'ease' instead of the traditional 'reef' and 'flat', showing that these two new parameters allows estimation of the boat velocity within an accuracy of $\pm 1\%$, while 'reef' and 'flat' under-estimates the boat velocity by up to 4%.

Similar heeling systems were adopted in Auckland and Valencia. The hull is immersed in a water tank and connected by three pins to a balance underneath the floor (Fig. 9). An electric motor drives an actuator, which heels the model. The water allows the clearance between the model and the floor to be sealed for all heel angles.

The balance used at the Politecnico di Milano Wind Tunnel is different, consisting of a self-contained prism which is placed inside the model (Fig. 10). The floor presents a minimum clearance, which can eventually be closed by a thin flexible membrane (lower insert in Fig. 10). The balance is placed on top of a rotating frame heeled by an electric motor (upper insert in Fig. 10).

2.5 SAIL SHAPE DETECTION

The twisted flow wind tunnels in Auckland, Kiel and Milan have all introduced flying shape detection systems in the last five years. Every sail trim is recorded and used to correlate measured forces with sail shapes. The geometries are also used to perform CFD analysis.

Sail shape detection has allowed a step change in the understanding of sail aerodynamics. When different sails are tested, these are trimmed independently to each other and, therefore, the resulting aerodynamic forces not only reflect different sails, but also reflect different trims. Sail shape detection allows investigation of which changes in the sail shape and trim lead to which changes in the aerodynamic forces. Moreover, when a test is repeated, flying shape detection allows verification that the same sail trim is actually achieved. This is very important in order to verify the setup of the experimental procedure and to monitor undesired deformations of the sailcloth.

Importantly, flying shape detection allows modelling of the experimental tests with CFD. Wind tunnel tests and CFD are two complementary research tools, which can be used effectively to investigate different aspects of sail aerodynamics. In fact, using flexible sails, the aerodynamic forces correlated with different sail trims can be effectively measured with wind tunnel tests. Differently, surface pressures are measured with difficulty on flexible sails due to the weight and size of the pressure taps (see Section 4.1); and the flow field is measured with difficulty in highly-turbulent boundary-layer wind tunnels. Conversely, as discussed in Section 3, CFD is very effective in computing the flow and pressure fields around rigid sails, while modelling different sail trims requires the coupling with a structural code, leading to a significant increase in the level of difficulty and uncertainty.

The first applications of flying shape detection were developed almost simultaneously in 2006 at the YRU of Kiel [21] and at the Politecnico di Milano Wind Tunnel [19,22], where up to eight high-frequency infrared cameras were used to record simultaneous images of markers positioned on the sails. In order to enhance the accuracy of the measurement, each marker needs to be recorded by the largest possible number of cameras simultaneously, thereby allowing accuracies of better than a tenth of a millimetre. The limitation of these systems is the cost of the hardware, and today they are rarely used.

The Twisted Flow Wind Tunnel in Auckland has a different system, namely VSPARS [23]. Only one camera per sail is used and horizontal stripes are detected. The main dimensions of each sail and of each stripe are provided *a-priori* to the software, which recognises the stripes in the picture and computes their positions. Figure 11 shows a typical photograph of an upwind sail taken from the model-scale yacht deck and processed by VSPARS. The system is not as accurate as the photogrammetric technique but its simplicity enables a fast setup and it is low in cost. In particular, the mid-section camber of mainsails, headsails and spinnakers are measured with an uncertainty of 0.5%, 1% and 2%, respectively [23]. The same system can be used at both the model scale and full scale. The camera is placed inside the model in the wind tunnel and can be placed in the same position on the deck of a full-scale yacht, allowing a high correlation between experiments and reality.

2.6 DYNAMIC TESTS

In the last few years, several tests have been performed to identify the aerodynamic coefficients in dynamic conditions. This is in part, to respond to the growing use of dynamic VPP, where a yacht's performance is also computed during the tacks (when the yacht turns its bow through the wind, such that the wind direction changes from one side of the boat to the other) and gybes (when the yacht turns its stern through the wind).

Dynamic VPP's mostly use aerodynamic coefficients measured in wind tunnels at the apparent wind angles that are sailed on a straight course, while they suffer from a lack of data for those very small apparent wind angles which are sailed only when tacking. Recently, these aerodynamic coefficients were measured by Gerhardt *et al.* [24], who used a quasi-steady approach for stepwise changes of the apparent wind angle.

Banks *et al.* [25] adopted a dynamic approach to measure the aerodynamic forces during the gybe, modelling the sails collapsing on one side and filling on the opposite side. The boat was placed on a turntable which rotated with a constant angular velocity, while the sails were remotely trimmed and the aerodynamic forces were measured.

Fossati and Muggiasca [26] were interested in the effect of the pitch angular motion on the aerodynamic forces when a boat sails into head waves. The aerodynamic forces show an hysteresis loop with the instantaneous apparent wind angle, which varies with the pitch angular velocity. The shape of the hysteresis loops, and therefore the amount of energy that is transferred to the sail, depends on the non-dimensional *reduced velocity* (apparent wind velocity divided by pitching frequency and sail chord) experienced by the sails. In previous work, Fossati and Muggiasca [27] also provided a rheological model based on springs, dampers, Coulomb friction elements, bump stops, etc. that allowed the aero-elastic forces to be computed. Fortunately for those researchers that neglect these dynamic effects, the centres of the hysteresis loops are quite well approximated by the quasi-static aerodynamic coefficients.

2.7 TWISTED FLOW WIND TUNNELS

There are three wind tunnels in the world where sails are regularly tested and a twisted flow device is used. These are the Twisted Flow Wind Tunnels of the YRU of Auckland and Kiel, and the Politecnico di Milano Wind Tunnel.

The YRU at the University of Auckland was established by Professor Peter Jackson in 1987 in response to the keen interest in yacht research generated by the University's involvement in New Zealand's first AC challenge in Fremantle, Australia. The wind tunnel was built in 1994 to support Team New Zealand in the 1995 AC challenge in San Diego. The Wind tunnel was built with the support of the University of Auckland, North Sails and Team New Zealand. The tunnel was relocated in 2005 to a different building and it has been continuously upgraded ever since. For instance, in 2010, the twisted flow device was rebuilt using some technological solutions introduced with the twisted vane device at the Politecnico di Milano; the electric motor used to heel the model was replaced with a faster one; the Real-Time VPP has been enhanced to take into account some features of the new VOR class; etc. The current tunnel is an open jet with a test section 7 m wide and 3.5 m high. The maximum speed is 8.5 m/s.

Wind tunnel tests were performed for many AC teams (Team New Zealand, 1995, 2000, 2003, 2007; BMW Oracle Racing, 2007; Alinghi, 2007; and Shosholoza, 2007), VOR teams (Illbruck Challenge, Assa Abloy, Team Tyco, News Corp, Team SEB and Djuice Dragons in 2001-2002: ABN Amro, Brazil 1, Movistar and Ericsson Racing Team in 2005-2006; other confidential teams in the current edition), and many other sailing teams.

The YRU of Kiel is a commercial spin-off of the University of Applied Sciences Kiel and came into being in 2000. Its tunnel was built in 2005 and it is the most recent of the three reviewed in this paper. The test section is 3.5 m wide and 2.4 m high, and the maximum velocity is 10 m/s. The balance, which was completely built in-house, presents interesting technological solutions allowing a high accuracy of the vertical forces. It is made of three CNC-milled thick layers of aluminium. The lowest layer is fixed to the ground via a vibration decoupling, the middle layer carries the fixed ends of the load cells and four water containers, whilst the highest layer leans on four bodies floating in the water and carries the model and the free ends of the load cells. Therefore, these floating bodies carry the weights of the upper layer and of the model, thereby providing hydrostatic release to the three vertically oriented load cells.

The Politecnico di Milano Wind Tunnel is the largest of the three, and is different from the others in that it is only partially used for sail aerodynamics. It was built in 2001 in a brand new building, belongs to the Politecnico di Milano and is used mainly by the Mechanical and the Aerospace Departments. Both these departments have performed wind tunnel tests for sailing teams. In particular, the former undertook tests for Prada challenger for the 31st AC, Luna Rossa challenger for the 32nd AC, and BMW Oracle Racing challenger for the 33rd AC.

The wind tunnel is a closed circuit with a large boundary-layer test section 14 m wide and 4 m high, and has a high-speed test section 4 m wide and 3.8 m high. Sails are tested in the larger test section where the maximum speed is 16 m/s.

3. NUMERICAL METHODS

3.1 POTENTIAL FLOW

The early pioneering work date back to the late 1960s. Milgram [28,29] and Gentry [30,31], followed by others, introduced potential flow codes to solve sail aerodynamics, allowing streamlines to be visualised around sails. The commercially most successful application of potential flow codes in sail aerodynamics, is the vortex lattice program *Flow*, which was developed by Michael Richelsen [32] in the 1980s for the sail making firm North Sails Inc. He also developed a finite-element program, *Membrain*, which computes the displacement of sails under the pressure distributions computed by *Flow*. *Flow* and *Membrain* are still the two most popular computer programs used by sail designers.

The potential-flow approach is still also used in the research field. For example, Spenkuch *et al.* [33] investigated the wake effect (known as the blanketing effect) of one boat on another during fleet races; Gerhardt *et al.* [34] studied the dynamic effect of pitching in waves on the aerodynamic sail's coefficient; and Pilate *et al.* [35] developed an "inverse" code able to compute the sail geometry given the desired pressure distribution. Potential-flow theory is also used by most VPPs to model how the sail coefficients vary with the sail trim (for example, see ref. [36]). However, in recent years, VPP's have made more and more use of regression formula fitting for experimental data: Claughton *et al*. [37] presented the recent changes to the International Measurement System VPP in the computation of induced drag and centre of effort, and both Claughton *et al.* [37] and Hansen *et al*. [20] have presented new models for the computation of the aerodynamic sail coefficients of different sail trims.

The limitation of using potential flow codes is the inability to model those conditions where flow separation is significant, such as in upwind conditions for tight trims (light air), and in downwind conditions (any wind speed).

3.2 REYNOLD-AVERAGED NAVIER-STOKES (RANS)

In numerical sail aerodynamics, a step change occurred in the 1990s with the first applications of RANS codes to downwind sails [38] followed by their application to upwind sails [39]. For the first time, RANS allowed the computation and the visual representation of separated flow. It is interesting to note how the grid resolution has increased from 1996 [38], where the number of grid points of the order of one thousand were used, to 2008 [40], where more than one billion cells were utilised. Between the various studies where the flow field was computed with RANS and the computed aerodynamics forces were validated with wind tunnel tests, it is worth mentioning the parametric studies on downwind sails by Lasher and Richards [41] and Lasher and Sonnenmeier [42], which allowed the correlation of the sail geometry with the flow field and sail coefficients.

In the last ten years, several authors (for instance, see refs. [43,44]) have coupled finite element structural codes with a RANS solver, and achieved the so-called *virtual wind tunnel*. The displacements are computed by a finite-element structural code, while the finite-volume RANS solver computes the pressure distributions. These codes are in continuous development, though the major challenge that they face is the current inability to perform a reliable validation of the results with experimental data.

RANS can be used with difficulty for those optimisation algorithms that require testing of a large number of geometries. For instance, Doyle *et al.* [45] used RANS with an evolutionary algorithm and with a gradient-based algorithm. In order to decrease the computational time, two-dimensional simulations were performed with a one-equation turbulence model. A much coarser grid was adopted by Chapin *et al.* [46] in order to use a three-dimensional model, and a one-equation turbulence model, with an evolutionary algorithm.

The major limitations of the RANS approach is the lack of generality of the turbulence model, which leads to difficulties in modelling some of the key features of sail aerodynamics. In particular, headsails and spinnakers have a sharp leading edge that leads to separation on the suction side of the sail. Laminar-to-turbulent transition occurs in the separated shear layer, enhancing the flow mixing process and bringing high-momentum fluid from the free stream to the near-wall region. This allows the flow to reattach despite the adverse pressure gradient, and forms the so-called laminar separation bubble [47]. Experiments on flat plates showed that vortices are shed periodically from the sharp leading edge and are convected along the shear layer, which immediately becomes unstable [48]. It was found that steady RANS under-estimate the mixing process, which, in the experiments, is enhanced by the unsteady flapping of the shear-layer. As a consequence, RANS tends to over-predict the laminar separation bubble length [49]. Also, two-equation turbulence models, such as $k - \omega$ and Shear- Stress Transport, which model the Reynolds stress tensor with an isotropic turbulence viscosity, fail to transfer the stream-wise kinetic energy generated in the shear layer to the span-wise and chord-wise velocity components at the reattachment point, lead to a slower recovery of the reattached boundary layer compared to experiments [49].

A different type of laminar separation bubble also occurs on both the suction and pressure side of the mast-mainsail, where the flow separates on the mast and reattaches on the sail. The pressure distribution corresponds to a laminar separation bubble, and the characteristics of the reattached turbulent boundary layer depend on where the laminar-to-turbulent transition occurs. Unfortunately, transition cannot be predicted with accuracy when using RANS, and therefore neither can the leading edge flow field. In addition, RANS models experience difficulties in modelling trailing edge separation on curved surfaces in high lift conditions.

Finally, Lasher and Richards [41] showed that two-equation turbulence models cannot be tuned to accurately model both the atmospheric boundary layer and the sail's boundary layer concurrently. In fact, as observed by Richards and Hoxey [50], the ratio between the turbulent kinetic energy and the square of the friction velocity is implicitly set by the constants of the turbulence model (for instance by the coefficient C_μ in the $k-\varepsilon$ model), resulting in much smaller values than those observed in the atmospheric boundary layer. Interested readers can find a discussion on the appropriate boundary conditions to model the atmospheric boundary layer in wind engineering applications, which include sail aerodynamics, in the recent paper by Richards and Norris [51].

In conclusion, even though RANS has allowed a step change in the understanding of sail aerodynamics, it is foreseeable that more advanced numerical techniques will overtake RANS in the future.

3.3 ADVANCED NUMERICAL TECHNIQUES

In other applications, such as aeronautics, Detached Eddy Simulations (DES) are becoming more and more popular, while only a few attempts have been made in the field of sail aerodynamics. Braun and Imas [52] stated that DES was used in the design process of an ACC-V5 yacht for the 32nd AC; however no results were presented, whilst Wright *et al.* [53] presented a DES simulation but no details were provided to verify the validity of the simulation. The authors found that DES allowed a greater insight on the effect of the velocity and pressure fluctuations on the mean flow, though this required a much higher grid resolution, and more importantly, a high grid regularity. In fact, DES employs RANS in the near-wall region and a Large Eddy Simulation (LES) in the outer region, and LES requires a much higher grid resolution than RANS [54].

More research is needed on the use of DES in sail aerodynamics, though the use of RANS in the near wall region leaves unresolved most of the limitations of a fully RANS approach. Conversely, the use of a fully LES approach would overcome these limitations and allow new insights into the unsteady near-wall flow features.

3.4 VERIFICATION AND VALIDATION

While performing verification and validation (V&V) of numerical simulations has become common practice in several fields, this is a very rare practice in sail aerodynamics. One of the reasons for this inexcusable lack of V&V is the difficulty until recently, in retrieving valuable experimental benchmarks. In fact, validation was only made possible for global force measurements via recent pressure measurements [55,56], which allowed a step change in the degree of validation: from a global parameter, such as the forces, to a local parameter, such as the pressure distributions. In the future, flow measurements will allow a further ground-breaking step change in the level of validation of numerical simulations.

General guidelines for V&V in CFD are provided by the American Society of Mechanical Engineers [57] while guidelines dedicated to marine applications are provided by the International Towing Tank Conference [58] and specialist guidelines for sail aerodynamics can be found in ref. [59]. Experimental data can be found in ref. [60] and refs. [41,42] to validate aerodynamic forces in upwind and downwind conditions, respectively, while pressure distributions can be found in ref. [56].

4. FULL-SCALE TESTS

4.1 FORCE MEASUREMENTS

In the 1990s several full-scale force measurements were performed, allowing a gain in confidence in the correspondence between wind tunnel tests and reality. Milgram *et al.* [61], on the 35-foot yacht *Amphetrete,* used an instrumented framework structure connecting the rigging to the hull with a six-component balance. The authors were able to measure the aerodynamic forces in equilibrium with the hydrodynamic forces. Similar concepts were developed by Masuyama and Fukasawa [62] and, successively, by Hochkirch and Brandt [63], on the 33-foot yachts *Fujin* and *Dyna*, respectively. Masuyama *et al.* [64] compared the aerodynamic forces measured on *Fujin* with those measured in a wind tunnel and adopted by the VPP of the International Measurement System (IMS), and as predicted by numerical codes. In particular, both a RANS code and a Vortex Lattice Method (VLM) were used to model the sail's flying shape recoded with on-board cameras. Figure 12 shows the lift and drag coefficients measured for the full scale yacht and computed numerically versus the apparent wind angle. The experimental measurements were performed both on port and a starboard tacks. In addition, two different headsails were used: a larger genoa (Fig. 12A) and a smaller jib (Fig. 12B). The sail coefficients in Fig. 12 show the good agreement between the full-scale measurements and the numerical simulations.

While Masuyama *et al.* [64] were focused on upwind conditions, Hansen *et al.* [65] compared the aerodynamic forces measured for a wider range of apparent wind angles on *Dyna* with those measured in a wind tunnel. The authors found poorer agreement than Masuyama *et al.* [64], perhaps due to the very large dispersion of the experimental data.

Augier *et al.* [66] used several load and position sensors on a J80-class yacht to study the unsteady fluid-structure interaction in real sailing conditions. They found that the loads on the rigging show hysteresis loops with the pitch motion of the boat, in agreement with the wind tunnel tests performed by Fossati and Muggiasca [26].

4.1 PRESSURE MEASUREMENTS

The first attempt to measure full-scale pressure distributions on sails was conducted by Warner and Ober [67] in the 1920s, who measured the pressures on a few sections of a full-scale C-class yacht mainsail and headsail. Unfortunately, the authors were unable to record the flying shapes of the sails, and thus the correlation between geometries and pressure distributions is unknown. After this outstanding and pioneering study, pressures were measured only in wind tunnels until much more recently. Marchaj [68] presented the first pressure distributions of a mainsail measured in a wind tunnel, but no information on the geometry and the flow conditions were provided. In the 1980s, Wilkinson [69] measured the pressure distributions on two-dimensional mast/mainsail sections in a wind tunnel. His work has been the only available benchmark for sail pressures until recently.

Modern full scale pressure measurements were unsuccessfully attempted by Flay and Millar [70], who reported the lessons they had learned. The sailing team BMW Oracle, challenger of the 32nd AC, measured the pressures at a few locations on the mainsail of an AC yacht [71]. Unfortunately, the pressure taps were too few to describe the pressure distributions on the sail. In contrast, Puddu *et al.* [72] successfully measured the pressure distributions on several sections of a full-scale mainsail of a Tornado-class catamaran. Since these initial works, several pressure measurements have been performed both in full scale and model scale. Richards and Lasher [55], and Viola *et al.* [56] measured the first pressure distributions on a model-scale spinnaker and headsail respectively. Both these works include the comparison with the pressures computed with CFD.

Viola and Flay [5] summarised the most recent pressure measurements and compared the pressures measured on-water in full-scale, with a wind tunnel model-scale, and numerically with CFD. The authors found that the flow field in the wind tunnel is well correlated with the full-scale flow field, although a few differences were noted. Downwind sails, which have a free leading edge, tend to be trimmed tighter in real sailing conditions than in a wind tunnel, where the onset flow can be controlled and the sails can be trimmed closer to the condition where the leading edge would collapse. For example, Fig. 13 shows a downwind sail tested both in full-scale on the water and in model scale in a wind tunnel. The pressure coefficient C_p is defined in Eq. (18), where p is the local surface pressure, and p_∞ is the far field pressure. Figure 13 shows the C_p measured on the leeward side of the sail versus the normalised curve length of three horizontal sections at $1/4$th, $1/2$nd and $3/4$th of the sail height respectively.

$$C_p = \frac{p - p_\infty}{q_\infty} \tag{18}$$

The full-scale and model-scale tests were performed at slightly different apparent wind angles: 70° and 80°, respectively. In both experiments the sails were trimmed in order to maximise the drive force. The full-scale and model-scale C_p ranges are between the same values for the three sections. However, the single suction peak measured in the full scale yacht indicates that the sail is trimmed to a tighter trim than at the model scale.

5. CONCLUSIONS

This paper presents the state of the art of sail aerodynamics and reviews the most important breakthroughs of the last 15 years. A yacht is designed using a program that computes the equilibrium of the aerodynamic and hydrodynamic forces and moments, namely a VPP. More and more often these programs also take into account the dynamic behaviour of the yacht, such as tacking and jybing. The aerodynamic forces are modelled by means of aerodynamic coefficients, which can be identified through wind tunnel tests or CFD.

In wind tunnel tests, a devoted device twists the onset flow in order to model the vertical velocity profile experienced by a sailing yacht. Flexible sails allow the investigation of a wide range of realistic sail trims in a short period of time, and a Real-Time VPP is included in the measurement system to heel the yacht during the test, allowing the sails to be trimmed and the boat to reach maximum speed. Flying shape detection systems are commonly used, allowing the same trim tested experimentally to be modelled numerically. The main limitation of wind tunnel tests is that the full-scale *Re* numbers cannot be reached due to the fragility of the model.

While potential flow codes are still widely used for upwind sails, RANS codes are commonly used for downwind sails. Both these codes need to be coupled with finite element structural codes in order to be able to identify the optimum sail trim. However, these coupled programs are difficult to validate and more research is needed in this area. The growth of computational resources has allowed several pioneering attempts to be made regarding optimisation with evolutionary algorithms using RANS codes, and more are expected in the future. Wider use of more advanced numerical methods, such as DES and LES, are also expected to be undertaken. In particular, LES will allow the modelling of peculiar unsteady flow features of sail aerodynamics, gaining new insights on the effect of transition on the laminar separation bubble and the evolution of the reattached boundary layer until trailing edge separation occurs.

At full-scale, the uncontrolled onset flow conditions lead to low measurement accuracy. However, experiments performed in recent years have shown that the aerodynamic forces and the pressure distributions measured on the water are not dissimilar from those measured in a wind tunnel. More significant differences were noted in downwind conditions, where the uncontrolled real onset flow leads to tighter sail trims than those modelled in wind tunnels and used to design sails.

Wind tunnel techniques, numerical methods and full-scale experiments, have all experienced a remarkable growth in the past 15 years and have demonstrated growing agreement between their findings.

6. ACKNOWLEDGMENTS

This article could have not have been written without the support that the author has received during his career from two exceptional people: Emeritus Fellow Mr Ian Campbell and Prof. Richard Flay. Ian has recently step down as Director of the Wolfson Unit at the University of Southampton after 38 years of service, while Richard was Director of the Yacht Research Unit at the University of Auckland from 1992 to 1998, and then again since 2007. The exceptional value of these two persons is matched by the greatness of their two research units.

7. REFERENCES

[1] Claughton, A.R., Wellicome, J.F., Shenoi, R.A., 2006, "Sailing Yacht Design: Theory," 2nd revised edition. University of Southampton, Computing Service, Southampton, UK, ISBN-10: 0854328297.

[2] Larsson, L., Eliasson, R.E., 2007, "Principles of Yacht Design," 3rd Edition. Adlard Coles Nautical, ISBN-10: 0713678550.

[3] Van Oossanen, P., 1993, "Predicting the Speed of Sailing Yachts," SNAME Trans., 101, pp. 337-397.

[4] Mirzaei, P.A., Rad, M., 2012, "Toward Design and Fabrication of Wind-Driven Vehicles: Procedure to Optimize the Threshold of Driving Forces," Applied Mathematical Modelling, in press.

[5] Viola, I.M., Flay, R.G.J., 2011, "Sail Pressures from Full-Scale, Wind-Tunnel and Numerical Investigations," Ocean Eng., 38, pp. 1733-1743.

[6] Querard, A.B.G., Wilson, P.A., 2007, "Aerodynamic of Modern Square Head Sails: a Comparative Study Between Wind-Tunnel Experiments and RANS Simulations," Proc. The Modern Yacht, October 11th-12th, Southampton, UK.

[7] Fossati, F., Muggiasca, S., Viola, I.M., 2006, "An Investigation of Aerodynamic Force Modelling for IMS Rule Using Wind Tunnel Techniques," Proc. 19th HISWA Symposium on Yacht Design and Yacht Construction, November 13th-14th, Amsterdam, The Netherlands, pp. 49-90.

[8] Campbell, I.M.C., 1997, "Optimisation of a Sailing Rig using Wind Tunnel Data," Proc. 13th Chesapeake Sailing Yacht Symposium, January 25th, Annapolis, MD, pp. 49-63.

[9] Flay, R.G.J., 1996, "A Twisted Flow Wind Tunnel for Testing Yacht Sails," J. of Wind Eng. and Ind. Aerody., 63, pp. 171-182.

[10] Hansen, H., Richards, P.J., Hochkirc, K., 2005, "Advances in the Wind Tunnel Analysis of Yacht Sails", Proc. 26th Symposium on Yacht Design and Construction, November 4th-5th, Hamburg, Germany.

[11] Viola, I.M., Flay, R.G.J., 2010, "Pressure Distribution on Modern Asymmetric Spinnakers", Int. J. of Small Craft Tech., Trans. RINA, 152(B1), pp. 41-50.

[12] Zasso, A., Fossati, F., Viola, I.M., 2005, "Twisted Flow Wind Tunnel Design for Testing Yacht Sails," Proc. 4th European and African Conference on Wind Engineering (EACWE4), July 11th-15th, Prague, Czech Republic.

[13] Graf, K., Mueller, O., 2005, "Der Twist-Flow-Windkanal der Yacht Research Unit Kiel," Proc. 25th Symposium Yacht Design and Yacht Construction, November, Hamburg, Germany.

[14] Le Pelley, D., Ekblom, P., Flay, R.G.J., 2002, "Wind Tunnel Testing of Downwind Sails", Proc. 2nd High Performance Yacht Design Conference, February 14th-16th, Auckland, New Zealand.

[15] Zasso, A., Fossati, F., Viola, I.M., 2005, "Twisted Flow Wind Tunnel Design for Testing Yacht Sails", Proc. 4th European and African Conference on Wind Engineering (EACWE4), July 11th-15th, Prague, Czech Republic.

[16] Cooper, K.R., 1991, "The Wind Tunnel Simulation of Wind Turbulence for Surface Vehicle Testing", J. Wind Eng. Ind. Aerodyn., 38, 71-81.

[17] Flay, R.G.J., Stevenson, D.C., 1988, "Integral Length Scale in Strong Winds Below 20 m", J. Wind Eng. Ind. Aerodyn., 28, 21-30.

[18] Hansen, H., Jackson, P.S., Hochkirch, K., 2003, "Real-Time Velocity Prediction Program for Wind Tunnel Testing of Sailing Yachts," Proc. The Modern Yacht, Southampton, UK.

[19] Fossati, F., Muggiasca, S., Viola, I.M., Zasso, A., 2006, "Wind Tunnel Techniques for Investigation and Optimization of Sailing Yachts Aerodynamics," Proc. 2nd High

Performance Yacht Design Conference (HPYD2), February 14th-16th, Auckland, New Zealand, pp. 105-113.

[20] Hansen, H., Richards, P.J., Jackson, P.S., 2010, "Reef and Flat or Twist and Ease: an Improved Trim Parameter Model for Yacht Sails," Int. J. of Small Craft Tech., RINA Trans., 152(B1), pp. 9-20.

[21] Renzsch H., Graf K., Müller O., 2006, "Strömungssimulation und Windkanalexperiment für die Analyse von Vormwind-Segeln," Proc. 26th Symposium Yacht Design and Yacht Construction, November, Hamburg, Germany.

[22] Martina, F., 2009, "Rilievo della geometria e del movimento dei corpi investiti da una vena fluida," Ph.D. thesis, Politecnico di Milano, Italy.

[23] Le Pelley, D.J., Modral, O., 2008, "V-Spars: A Combined Sail and Rig Shape Recognition System Using Imaging Techniques," Proc. 3rd High Performance Yacht Design Conference Auckland, December 2nd-4th, pp. 57-66.

[24] Gerhardt, F.C., Le Pelley, D., Flay, R.G.J., Richards, P., 2009, "Tacking in the Wind Tunnel," Proc. 19th Chesapeake Sailing Yacht Symposium, March 20th-21st, Annapolis, MD, pp. 161-175.

[25] Banks, J., Webb A., Spenkuch T., Turnock S.R., 2010, "Measurement of Dynamic Forces Experienced by an Asymmetric Yacht During a Gybe, for use within Sail Simulation Software," Procedia Eng. 2(2), pp. 2511-2516.

[26] Fossati, F., Muggiasca, S., 2011, "Experimental Investigation of Sail Aerodynamic Behaviour in Dynamic Conditions," J. of Sailboat Tech., pp. 2011-02.

[27] Fossati, F., Muggiasca, S., 2010, "Numerical Modelling of Sail Aerodynamics Behaviour in Dynamic Conditions," Proc. 2nd International Conference on High Performance Sailing Yachts, Lorient, France.

[28] Milgram, J.H., 1968, "The Aerodynamics of Sails," Proc. 7th Symposium of Naval Hydrodynamics, pp. 1397-1434.

[29] Milgram, J.H., 1968, "The Analytical Design of Yacht Sails," Porc. SNAME Annual Meeting, pp. 118-160.

[30] Gentry, A.E., 1971, "The Aerodynamics of Sail Interaction," Proc. 3rd AIAA Symposium on the Aero/Hydronautics of Sailing, Redondo Beach, CA.

[31] Gentry, A.E., 1988, "The Application of Computational Fluid Dynamics to Sails," Proc. Symposium on Hydrodynamic Performance Enhancement for Marine Applications, Newport, RI.

[32] Whidden, T., Levit, M., 1990, "The Art and Science of Sails," Adlard Coles Nautical, ISBN-10: 0229118887.

[33] Spenkuch, T., Turnock, S. R., Scarponi, M., Shenoi, A., 2011, "Modelling multiple yacht sailing interactions between upwind sailing yachts," J. of Mar. Sci. and Tech., 16(2), pp. 115-128.

[34] Gerhardt, F.C., Flay, R.G.J., Richards, P., 2011, "Unsteady Aerodynamics of Two Interacting Yacht Sails in Two-Dimensional Potential Flow," J. Fluid Mech., 668, pp. 551-581.

[35] Pilate, J.P., Gerhadt, F.C., Flay, R.G.J., 2010, "A Three-Dimensional Inverse Sail Design Method," Int. J. Small Craft Tech., Trans RINA, 152(B2), pp. 107-114.

[36] Jackson, P.S., 1996, "Modelling the Aerodynamics of Upwind Sails," J. of Wind Eng. And Ind. Aerodyn., 63, pp. 17-34

[37] Claughton, A., Fossati, F., Battistin, D., Muggiasca, S., 2008, "Changes and Development to Sail Aerodynamics in the ORC International Handicap Rule," Proc. 20th International Symposium on Yacht Design and Yacht Construction, November, Amsterdam, The Netherlands.

[38] Hedges, K.L., Richards, P.J., Mallison, G.D., 1996, "Computer Modelling of Downwind Sails," J. of Wind Eng. and Ind. Aerody., 63, pp. 95-110.

[39] Miyata, H., Lee, Y.W., 1999, "Application of CFD Simulation to the Design of Sails," J. of Mar. Sci. and Tech., 4, pp. 163-172.

[40] Viola, I.M., Ponzini, R., 2011, A CFD Investigation with High-Resolution Grids of Downwind Sail Aerodynamics," Proc. Developments in Marine CFD, March 23rd-24th, London, UK.

[41] Lasher, W.C., Richards, P.J., 2007, "Validation of Reynolds-Averaged Navier-Stokes Simulations for International America's Cup Class Spinnaker Force Coefficients in Atmospheric Boundary Layer," J. of Ship Research, 51(1), pp. 22-38.

[42] Lasher, W.C., Sonnenmeier, J.R., 2008, "An Analysis of Practical RANS Simulations for Spinnaker Aerodynamics," J. Wind Eng. and Ind. Aerodyn., 96, pp. 143-165.

[43] Richter, H.J., Horrigan, K.C., Braun, J.B., 2003, "Computational Fluid Dynamics for Downwind Sails," Proc. 16th Chesapeake Sailing Yacht Symposium, March, Annapolis, MD.

[44] Renzsch, H., Müller, O., Graf, K., 2008, "FLEXSAIL – A Fluid Structure Interaction Program for the Investigation of Spinnakers," Proc. International Conference on Innovations in High Performance Sailing Yachts, Lorient, France.

[45] Doyle, T., Gerritsen, M.G., Iaccarino, G., 2005, "Sail Shape Optimization of a Modern Clipper Yacht," Int. J. of Small Craft Tech., RINA Trans., 147 (B2).

[46] Chapin, V.G., de Carlan, N., Heppel, P., 2011, "A Multidisciplinary Computational Framework for Sailing Yacht Rig Design & Optimization through Viscous FSI," Proc. 20th Chesapeake Sailing Yacht Symposium, March 18th-19th, Annapolis MD.

[47] Viola, I.M., Flay, R.G.J., 2011, "Sail Aerodynamics: Understanding Pressure Distributions on Upwind Sails," Exp. Thermal and Fluid Sci., 35(8), pp. 1497-1504.

[48] Gault, D. E., 1957, "An Investigation at Low Speed of the Flow Over a Simulated Flat Plate at Small Angles of Attack Using Pitot Static and Hot-Wire Probes," NACA, Technical Report No. TN-3876.

[49] Collie, S., Gerritsen, M., Jackson, P., 2008, "Performance of Two-Equation Turbulence Models for Flat Plate Flows with Leading Edge Bubbles", J. Fluid Eng. – T. ASME, 130(2), pp. 0212011-02120111

[50] Richards, P.J., Hoxey, R.P., 1993, "Appropriate Boundary Conditions for Computational Wind Engineering Models Using the $k-\epsilon$ Turbulence Model", J. Wind Eng. Ind. Aerodyn., 46 and 47, 145–153.

[51] Richards, P.J., Norris, S.E., 2011, "Appropriate Boundary Conditions for Computational Wind Engineering Models Revisited", J. Wind Eng. Ind. Aerodyn., 99, 257–266.

[52] Braun, J.B, Imas, L., 2008, "High Fidelity CFD Simulations in Racing Yacht Aerodynamic Analysis," Proc. 3rd High Performance Yacht Design Conference, December 2nd-4th, Auckland, New Zealand.

[53] Wright, A.M., Claughton, A.R., Paton, J., Lewins, R., 2010, "Off-Wind Sail Performance Prediction and Optimisation," Proc. 2nd International Conference on Innovations in High Performance Sailing Yachts, Lorient, France.

[54] Spalart, P.R., 2009, "Detached Eddy Simulation," Annual Rev. of Fluid Mech., 41, pp. 181-202.

[55] Richards, P.J., Lasher, W., 2008, "Wind Tunnel and CFD Modelling of Pressures on Downwind Sails," Proc. VI International Colloquium on: Bluff Bodies Aerodynamics & Applications, July 20th-24th, Milan, Italy.

[56] Viola, I.M., Pilate, J., Flay, R.G.J., 2011, "Upwind Sail Aerodynamics: a Pressure Distribution Database for the Validation of Numerical Codes", Int. J. of Small Craft Tech., Trans. RINA, 153(B1), pp. 47-58.

[57] American Society of Mechanical Engineers (ASME), Standard for Verification and Validation in Computational Fluid Dynamics, ASME Committee PTC61, 2008, "ASME V&V 20-2009", Alexandria, VA.

[58] International Towing Tank Conference (ITTC), Recommended Procedures, Uncertainty Analysis in CFD, 2008, "Verification and Validation Methodology and Procedures (7.5-03-01-01)."

[59] Viola I.M., Bot P., Riotte M., 2013, "On the Uncertainty of CFD in Sail Aerodynamics", Int. J. for Numer. Meth. Fl., in press, DOI: 10.1002/fld.3780.

[60] Fossati, F., Martina, F., Muggiasca, S., 2008, "Experimental Database of Sail Performance and Flying Shapes in Upwind Conditions", Proc. International Conference on Innavation in High Performance Sailing Yachts, May 29th-30th, Lorient, France.

[61] Milgram, J.H., Peters, D.B., Eckhouse, D.N., 1993, "Modeling IACC Sail Forces by Combining Measurements with CFD," Proc. 11th Chesapeake Sailing Yacht Symposium, January 29th-30th, Annapolis, MD, pp. 65-73.

[62] Masuyama, Y., Fukasawa, T., 1997, "Full-Scale Measurements of Sail force and Validation of Numerical Calculation Method," Proc. 13th Chesapeake Sailing Yacht Symposium, January 25th, Annapolis, MD, pp. 23-36.

[63] Hochkirch, K., Brandt, H., 1999, "Full-Scale Hydrodynamic Force Measurement on the Berlin Sailing Dynamometer," Proc. 14th Chesapeake Sailing Yacht Symposium, January 30th, Annapolis, MD, pp. 33-44.

[64] Masuyama, Y., Tahara, Y., Fukasawa, T., Maeda, N., 2009, "Database of Sail Shapes versus Sail Performance and Validation of Numerical Calculations for the Upwind condition," J. Mar. Sci. Tech., 14, pp. 137-160.

[65] Hansen, H., Jackson, P.S., Hochkirch, K., 2003, "Comparison of Wind Tunnel and Full-Scale Aerodynamic Sail Force Measurements," Int. J. of Small Craft Tech., RINA Trans., 145(B1), pp. 23-31.

[66] Augier, B., Bot, P., Hauville, F., Durand, M., 2012, "Experimental Validation of Unsteady Models for Fluid Structure Interaction: Application to Yacht Sails and Rigs," J. Wind Eng. And Ind. Aerody., 101, pp. 53-66

[67] Warner, E.P., Ober, S., 1925, "The aerodynamics of Yacht Sails," Proc. 3rd General Meeting of the Society of Naval Architects and Marine Engineers, November 12th-13th, New York, NY.

[68] Marchaj, C.A., 1964, "Sailing Theory and Practice," Dodd and Mead, New York, NY.

[69] Wilkinson, S., 1984, "Partially Separated Flows Around 2D Masts and Sails," Ph.D. thesis, University of Southampton, UK.

[70] Flay, R.G.J., Millar, S., 2006, "Experimental Consideration Concerning Measurements in Sails: Wind Tunnel and Full Scale," Proc. 2nd High Performance Yacht Design Conference, February 14th-16th, Auckland, New Zealand.

[71] Gaves, W., Barbera, T., Braun, J.B., Imas, L., 2008, "Measurements and Simulation of Pressure Distribution on Full size scales," Proc. 3rd High Performance Yacht Design Conference, December 2nd-4th, Auckland, New Zealand.

[72] Puddu, P., Erriu, N., Nurzia, F., Pistidda, A., Mura, A., 2006, "Full Scale Investigation of One-Design Class Catamaran Sails", Proc. 2nd High Performance Yacht Design Conference, February 14th-16th, Auckland, New Zealand.

FIGURES

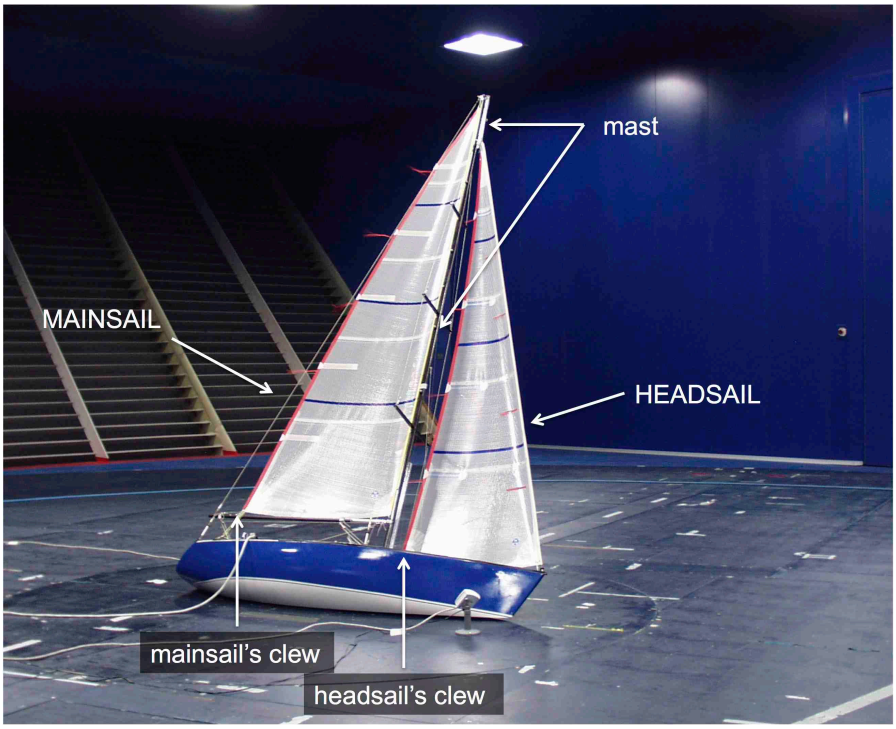

Figure 1: Example of a wind tunnel test in upwind conditions in the Politecnico di Milano Wind Tunnel

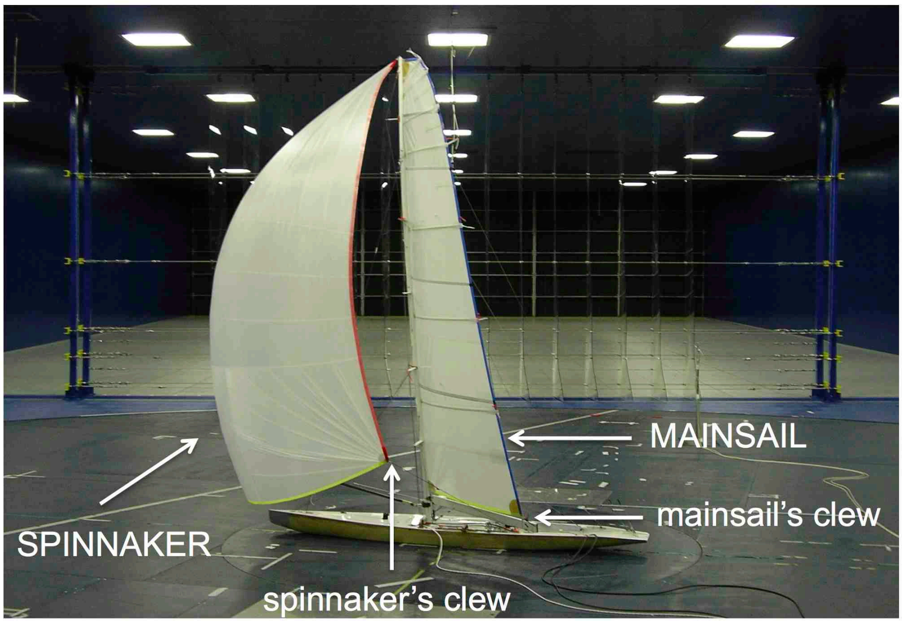

Figure 2: Example of a wind tunnel test in downwind conditions in the Politecnico di Milano Wind Tunnel

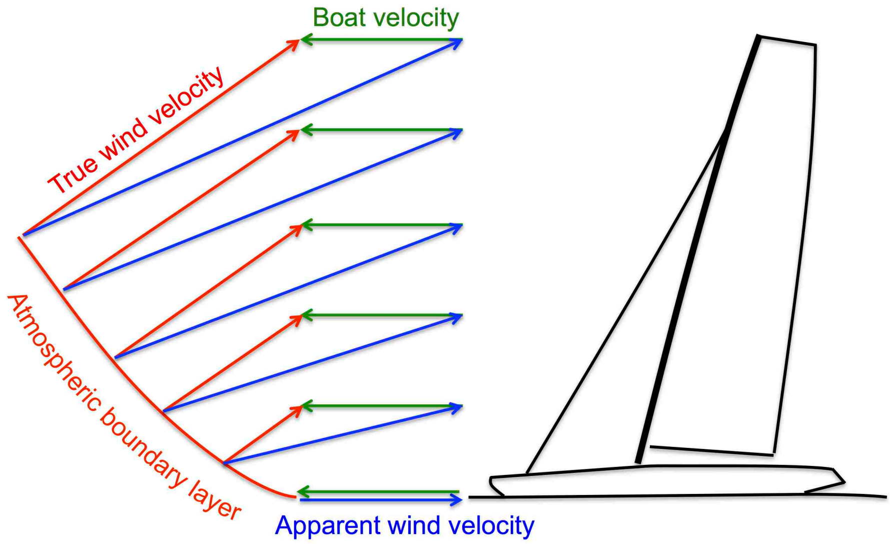

Figure 3: Wind Triangle

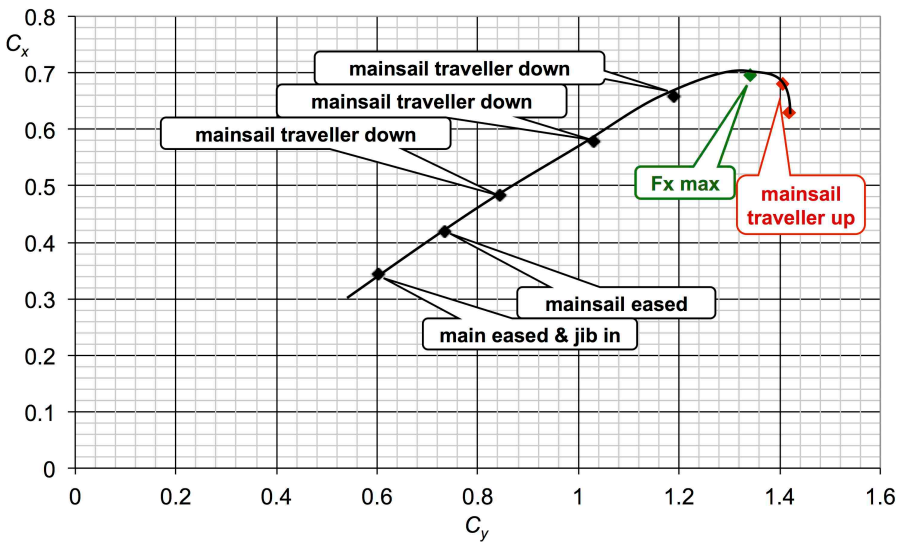

Figure 4: Drive force coefficient versus side force coefficient

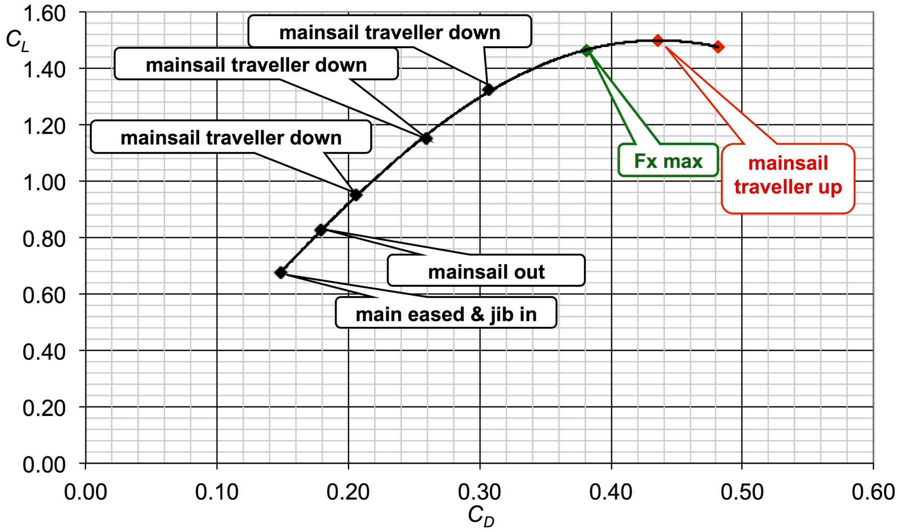

Figure 5: Lift coefficient versus drag coefficient

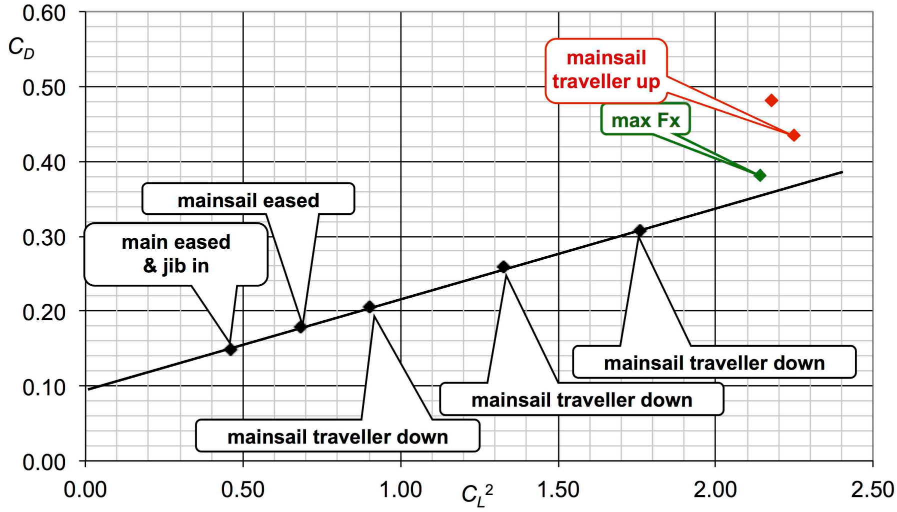

Figure 6: Drag coefficient versus lift coefficient squared.

Figure 7: Twisted Flow Wind Tunnel of the Yacht Research Unit, Auckland.


Figure 8: Twisted Flow Wind Tunnel of the Yacht Research Unit, Kiel.

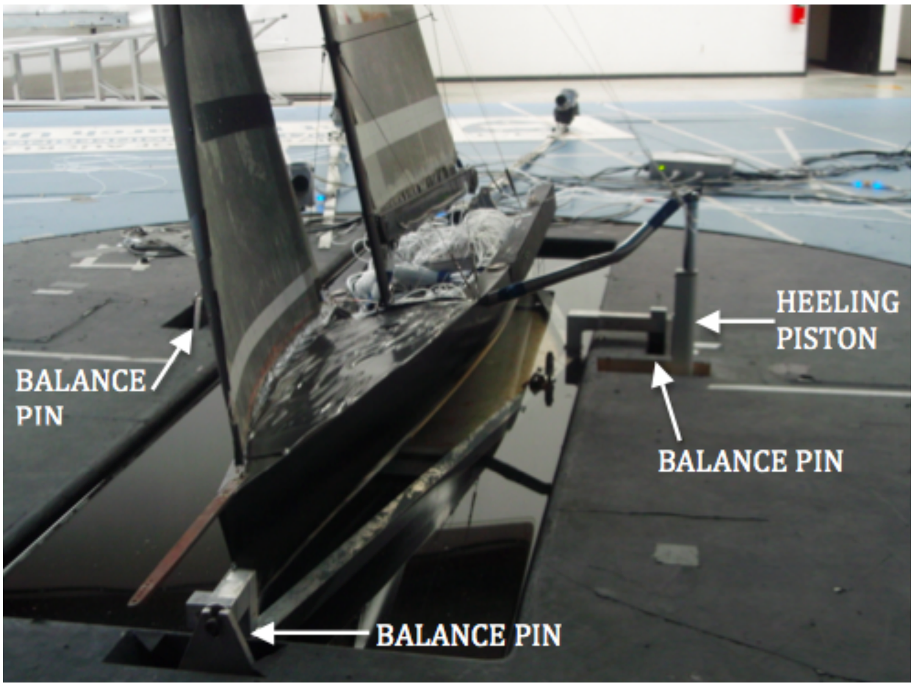

Figure 9: The model immersed in a water tank at the Twisted Flow Wind Tunnel of the Yacht Research Unit, Auckland.

Figure 10: Setup for the Real-Time VPP at the Politecnico di Milano Wind Tunnel and details of the balance on the rotating frame (top insert) and the boat-floor clearance closure (lower insert).

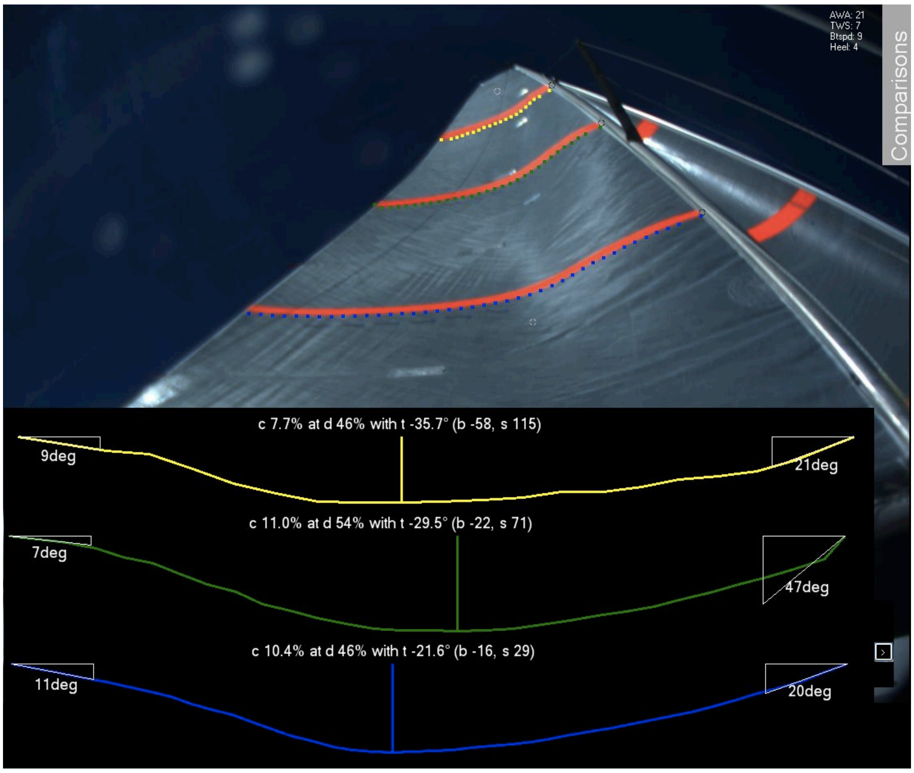

Figure 11: Typical photograph of a sail processed with VSPAR.

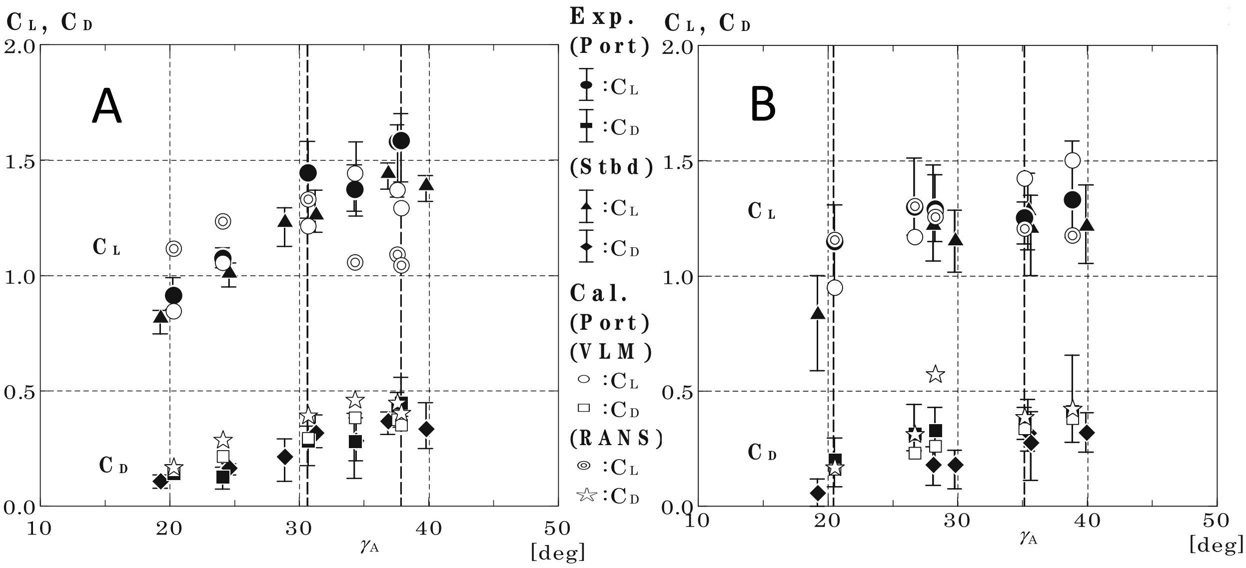

Figure 12. Lift and drag coefficients measured full scale (Exp.), computed with VLM and RANS, for a genoa (A) and a jib (B). Edited from Masuyama *et al.* [64].

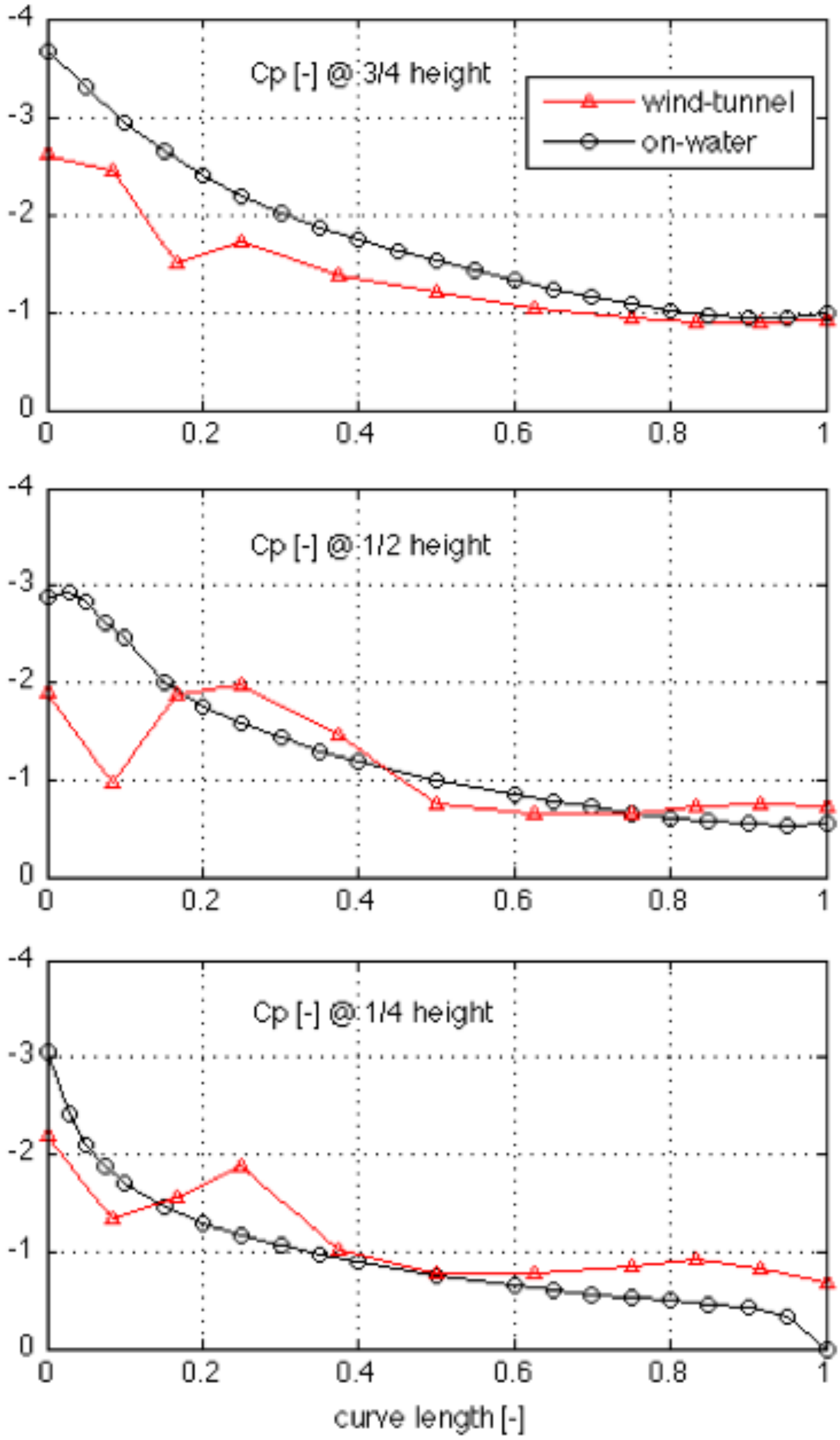

Figure 13: Full-scale and model-scale C_p on three sail sections.